GEOMORPHOMETRY 2025
PERUGIA ITALY JUNE 9-13

Assessing the morphological changes of a large landslide using high-resolution UAS and airborne LiDAR data

Manuel Stark[1], Annalisa Sannino[2] and Francesca Vergari[2] § correspondence to: Manuel Stark (mstark@ku.de)

[1]Department of Physical Geography,
Catholic University of Eichstätt-Ingolstadt
Eichstätt, Germany

[2]Department of Earth Sciences
Sapienza University of Rome
Rome, Italy

Abstract -- The Upper Orcia Valley exhibits a high geomorphological susceptibility to denudation processes, which manifest through continuous water erosion and the frequent occurrence of landslides, due to the high erodibility of its clay-rich marine and fluvial Pliocene deposits in a sub-humid environment. A significant landslide event occurred in January 2021 on a badland hillslope, affecting an area of 0.54 km² within the Formone sub-catchment, approximately 6 km northwest of the Radicofani village. The landslide occurred in a badland hillslope, marking a transition from water-driven denudation processes to gravitational mass movements, thus leading to a complete reconfiguration of the hillslope. This study aims to quantify the morphological changes induced by the landslide and analyze the erosion dynamics of complex landslides in clay-rich substrates. UAS photogrammetry (SfM-MVS), airborne LiDAR, and DGNSS surveys were employed to analyze volumetric changes over a decade (2012–2022), identify the most affected areas, and investigate the internal morphological evolution of the landslide. The results indicate a total displacement of 17302 m³ of material, with a maximum surface lowering of -6.49 m in the landslide scarp and a maximum deposition of +5.01 m in the westernmost section, resulting in a negative sediment balance of 9980 m³. The landslide, which exhibits a complex dynamic, evolved into a debris flow, with secondary erosion processes further reshaping the landscape. Given the region's susceptibility to denudation and anthropogenic modifications, understanding these processes is crucial for hazard assessment and mitigation strategies. This study highlights the importance of high-resolution topographic surveys for detecting morphological changes and evaluating landslide-prone areas in similar environments.

I. Introduction

The landscape Upper Orcia Valley in Tuscany (Italy) is distinguished by rapid denudation dynamics primarily attributable to the high erodibility of the lithological outcrops (clay-rich marine and fluvial Pliocene deposits). This morphodynamics is further intensified by the Mediterranean climate regime and steep slope gradients, resulting in widespread badlands, where water erosion is predominant and frequent landslides [1],[2],[3]. A notable example occurred in January 2021, when a significant landslide (0,54 km²) affected the Provinciale del Monte Amiata road between the villages of Contignano and Le Conie, causing road closure, damage to infrastructures (supply networks for electricity, gas and water) and disruptions to local residents [4]. This landslide took place on a badlands surface (locally called "calanchi") on which it developed, leading to a total reconfiguration of the hillslope. This study aims to examine and quantify the morphological change caused by this landslide. Therefore, advanced methods like UAS photogrammetry (SfM-MVS), airborne LiDAR and DGNSS are used. Key research questions include assessing volumetric changes (2012-2022), identifying areas with the most significant transformations and gaining more insights into the erosion dynamics of complex landslides in clay-rich substrate.

II. Study Site

The study area (Fig. 1) is located in the Formone catchment, about 6 km north-west of the village of Radicofani between 475 m

and 575 m a.s.l. It is part of the Radicofani basin, a NW-SE facing depression bordered to the east by the Cetona ridge and to the west by the ridge between Monte Amiata and Castell'Azzara. The topography is predominantly characterised by fluvial landscapes [5],[6]. The climatic conditions of the region are typically Mediterranean (annual mean temperature: 14° C; precipitation: ˜700 mm [7]. Rainfall amounts and intensities reach its peaks during the autumn and spring months.

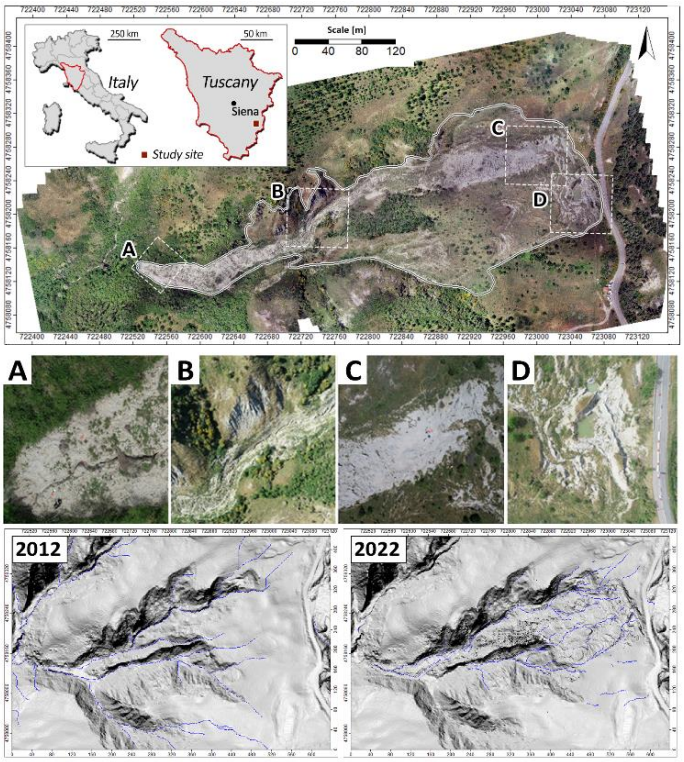

Figure 1, top: Study site with area of interest (AoI) with sub-regions (A-D) of the process area (middle). Bottom: Pre- and post-event hillshaded digital elevation model (DEM) 2012 (left) and digital terrain model (DTM) 2022. The blue lines show the respective main channel system.

III. Data Survey and Processing

A. Airborne LiDAR DTM

The airborne LiDAR data was acquired by the Ministry of the Environment and the Tutela del Territorio and del Mare as part of the Extraordinary Environmental Remote Sensing Plan [8] (resolution: 1 m). The data is available as digital elevation model DEM in a 1 m resolution.

B. Photogrammetric data & ground control points

Table 1 shows the main parameters of data survey. The ground control points (GCPs) were evenly distributed [9], at a distance of 15-80 m [10],[11] and measured with a DGNSS (Stonex S9III and S9i; rover-base-mode; accuracy: $9x10^{-3}$ m). DTMs (resolution: 0.2 m) and orthomosaics (resolution: 0.03 m) were than calculated using structure from motion and multi-view stereo (SFM-MVS) methods [12],[13]. A self-calibration was conducted for the camera parameters (cx, cy, k1, k2, k3, p1, p2), with the exception of the focal length, which was set to a pre-defined value (see table 1). The GCPs were incorporated to ascertain the exterior orientation of the data, (UTM Zone 32N; EPSG code: 25832). Subsequent to the completion of the SfM process, a 3D point cloud and an orthomosaic were calculated for each dataset. Following a comprehensive refinement of the point cloud, which included the filtering of outliers and poorly projected and reconstructed points. The photogrammetric DTMs were then resampled from 0.2 m resolution to 1 m (aggregation: lowest z-value corresponding to a grid cell) using a bilinear resampling tool [14].

C. Geomorphic change detection

Figure 2 shows the general workflow employed to ascertain the topographical changes. To distinguish real surface changes from noise the respective uncertainties need to be quantified. The individual DEM uncertainties can be estimated from repeated measurements or from unmodified, geomorphic stable areas (SA) [15]. As the survey design did not allow repeated observations, the SA approach was used to provide a level of detection (LoD) [16] as follows:

$$\sigma DoD = \Sigma_{mean}\, \sigma SA$$

where σDoD represent the mean of standard deviations of the height values of all stable area pixels in the DEM of Differences (DoD). We used a significance threshold at a critical t-value t crit of 1.96 from Student's t-distribution, corresponding to a confidence level of 95%. The level of detection (LoD) was calculated based on the following equation:

$$LoD = tcrit^{*}\, \sigma DoD \quad (tcrit=1.96)$$

The approach yielded a LoD of 0.18 m. Subsequent to the co-registration of the DTMs and accuracy analysis the DTMs recorded at two different points in time are utilised to calculate the height (surface) changes (DoD) and, consequently, the volume changes caused by the landslide. The DoD is calculated at a grid size of 1m (resolution of the airborne LiDAR DTM).

TABLE I. MAIN PARAMETER OF UAS SURVEY AND SFM-MVS POINTCLOUD

Date:	06/2022
Weather conditions:	dry / sunny
UAS / camera type & focal length:	Phantom 4 Pro + / 8.8 mm
Flight pattern:	Cross grid
Image overlaps (front- & sidelap):	85%
Image count:	1507
Flight altitude (above ground):	80 & 85 m
Point density:	424 p*m^{-1}
GCP count:	39
GCP RMSE:	0.03 m
Mean error/ std. dev. (stable areas):	-0.09 m/ 0.08 m

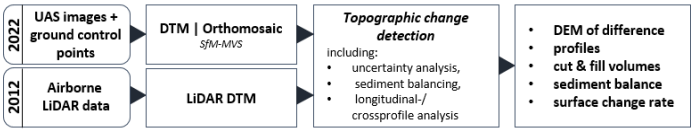

Figure 2: Workflow for UAS and LiDAR data processing and analysis.

IV. RESULTS AND DISCUSSION

The landslide caused a huge morphological change with an erosion volume of 17302 m³ and a deposition volume of 7322 m³ of material. This results in a total mass loss of 9980 m³ transported from the slope to the channel system and further downstream to the Formone River through runoff and other water-driven processes. The most pronounced surface variations occurred in the landslide scarp, in the uppermost part of the Area of Interest (AoI) west of the road, where the terrain subsided by up to -6.49 m (fig. 3). In contrast, the westernmost and lowest sections of the AoI experienced the greatest deposition, with a maximum surface increase of +5.01 m. Linear erosion has been observed to occur exclusively within the primary channel, characterised by gullying and piping, with maximum values reaching -2 m. This area is distinguished by the presence of highly erodible fine-grained material with a high clay content, and numerous subsurface channels on the so-called "popcorn surface," indicating an extensive drainage network piping enhanced after the landslide event, especially in the remolded deposition area. Overall, the event can be described as a complex landslide composed of distinct process zones, each exhibiting different forms of movement. The landslide is characterized by rotational movements in the upper scarp, as indicated by tilted power poles, transitioning into translational movements, mudflows, and gully formation processes in the lower sections. The landslide evolved downstream into a debris flow, particularly west of cross-profile *2 in figure 3, where steeper slopes (max. inclination of 52°) facilitated further material transport. The transport zone of the debris flow is defined by a narrow, incised channel with alternating gullying and piping. Furthermore, the unvegetated slopes north of the debris channel demonstrate a substantial erosion, exhibiting a pronounced slope-channel coupling (cross-profile 3 in figure 3).

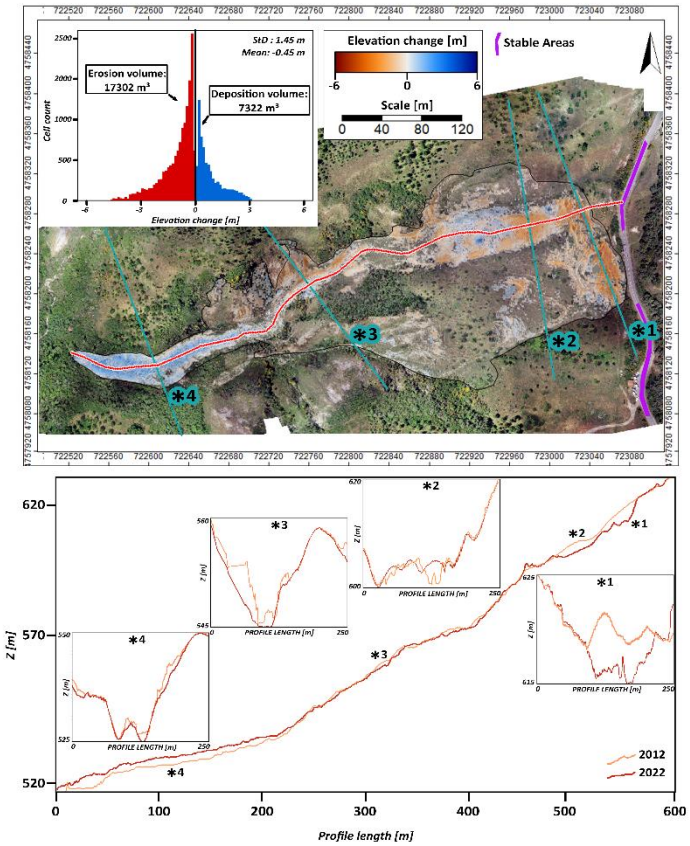

Figure 3: DoD with histogram, location of longitudinal-profile, cross-profiles (*1-*4) and stable areas.

According to the surface forms/process signatures, the changes were caused by a combination of shallow landslides and water-driven processes. The material eroded on the slopes was deposited directly on the depth contour after a transport distance of 5-20 metres from where the unconsolidated substrates can now be relatively easily displaced by secondary processes. In the north-western part of the study area, the main slide surface is characterized by significant rill formation (width: 5-60 cm/ depth: 2-40 cm), secondary scarps, and transversal cracks, all indicating ongoing secondary surface movements. The steep slopes in this area and the presence of large cracks suggest active surface processes and a potential future landslide event. The depth of the slide caused partial destruction of key infrastructure, including gas lines. Additionally, minor deposition zones acting as counter-slopes/dams led to the formation of small ponds and pools south of the central slide surface. Tilted power poles point towards rotational movements here and underlies the complexity of the landslide as it evolved into a debris flow further downstream.

North-westwards of a large, relatively flat area free of vegetation. The landslide on a badland surface reshaped the landscape, marking a transition from water-driven denudation to gravitational mass movements. This shift highlights how badlands landforms are prone to evolving through landslides supports the interpretation of the complex cause-effect relationship between calanchi and landslide occurrence in sub-humid climates [17]. Calanchi, which often initiate in landslide scars where vegetation has been removed, are then frequently affected by mass wasting. Future geomorphic processes will likely continue to reshape the landscape, particularly in unvegetated areas prone to secondary sub-events, primarily driven by water erosion on both hillslopes and within the channel network. With peak precipitation in spring and autumn, these seasons are expected to be the most geomorphically active, leading to the reactivation and further development of existing landforms, including the deepening or filling of rills and channels, the merging of erosional features, and the formation of new active spots [18]. As water erosion proceeds in basal channels, the fluvial domain could extend uphill, re-establishing the system functional sediment connectivity [17]. This could lead, in the near future, to the formation, again, of well-developed badlands in the landslide source area. Further studies on the evolution of dynamic sediment connectivity on this slope could enhance the accuracy of predicting its future development. Considering the natural predisposition of the area to denudation processes and anthropogenic modifications, a deeper understanding of these processes is crucial for early interventions and risk mitigation. Moreover, Structure-from-Motion Multi-View Stereo (SfM-MVS) photogrammetry has proven to be a valuable tool for detecting and quantifying landscape changes, especially at the catchment scale [7],[19].

References

[1] Della Seta, M., Del Monte, M., Fredi, P., Lupia Palmieri, E. (2009). Space–time variability of denudation rates at the catchment and hillslope scales on the Tyrrhenian side of Central Italy. *Geomorphology*, 107, 161–177. https://doi.org/10.1016/j.geomorph.2008.12.004

[2] Castaldi F., and Chiocchini U. (2012). Effects of land use changes on badland erosion in clayey drainage basins, Radicofani, Central Italy. *Geomorphology* 169–170, 98–108. https://doi.org/10.1016/j.geomorph.2012.04.016

[3] Vergari, F., Della Seta, M., Del Monte, M., Fredi, P., Lupia Palmieri, E. (2013a). Long- and short-term evolution of several Mediterranean denudation hot spots: the role of rainfall variations and human impact. *Geomorphology*, 183, 14–27. https://doi.org/10.1016/j.geomorph.2012.08.002

[4] Cherubini, D. (2021). Radicofani, nuova frana sulla Sp96 Il sindaco: "Ora è chiusa al traffico". In: La Nazione, January 21, https://www.lanazione.it/siena/cronaca/radicofani-nuova-frana-sulla-sp96-il-sindaco-ora-è-chiusa-al-traffico-1.5955089, accessed: 2023-02-09)

[5] Ciccacci, S., Galiano, M., Roma, M.A., Salvatore, M.C. (2008). Morphological analysis and erosion rate evaluation in badlands of Radicofani area (Southern Tuscany—Italy). *Catena*, 74, 87–97. https://doi.org/10.1016/j.catena.2008.03.012

[6] Vergari, F., Della Seta, M., Del Monte, M., Fredi, P., Lupia Palmieri, E. (2013a). Long- and short-term evolution of several Mediterranean denudation hot spots: the role of rainfall variations and human impact. *Geomorphology*, 183, 14–27. https://doi.org/10.1016/j.geomorph.2012.08.002

[7] Aucelli, P.P.C., Conforti, M., Della Seta, M., Del Monte, M., D'Uva, L., Rosskopf, C.M., Vergari, F. (2014). Multi-temporal digital photogrammetric analysis for quantitative assessment of soil erosion rates in the Landola catchment of the Upper Orcia Valley (Tuscany, Italy). *Land Degradation & Development*, 27(4), 1075-1092. https://doi.org/10.1002/ldr.2324

[8] 'DTM LiDAR with ground resolution 1 meter — Tuscany Region', 2013, accessed 2025-01-30, http://data.europa.eu/88u/dataset/m_amte-299fn3-6f2da530-bfde-4dfc-ba76-7e9bc3f8247f

[9] James, M.R., Robson, S. (2012). Straightforward reconstruction of 3D surfaces and topography with a camera: accuracy and geoscience application. *Journal of Geophysical Research: Earth Surface*, 117, F03017. https://doi.org/10.1029/2011JF002289

[10] Gindraux, S., Boesch, R., & Farinotti, D. (2017). Accuracy assessment of digital surface models from unmanned aerial vehicles' imagery on glaciers. *Remote Sensing*, 9(2), 186. https://doi.org/10.3390/rs9020186

[11] James, M.R., Robson, S., d'Oleire-Oltmanns, S., & Niethammer, U. (2017a). Optimising UAV topographic surveys processed with structure-from-motion: Ground control quality, quantity and bundle adjustment. Geomorphology, 280, 51–66. https://doi.org/10.1016/j.geomorph.2016.11.021

[12] Westoby, M.J., Brasington, J., Glasser, M.J., Hambrey, M.J., & Reynolds, J.M. (2012). Structure-from-Motion photogrammetry: a low-cost, effective tool for geoscience applications. *Geomorphology*, 179, 300–314. https://doi.org/10.1016/j.geomorph.2012.08.021

[13] Eltner, A. & Schneider, D. (2015). Analysis of different methods for 3D reconstruction of natural surfaces from parallel-axes UAV images. *The Photogrammetric Record*, 30(151), 279–299. https://doi.org/10.1111/phor.12115

[14] Conrad, O., Bechtel, B., Bock, M., Dietrich, H., Fischer, E.,Gerlitz, L., … Böhner, J. (2015). System for Automated Geoscientific Analysis (SAGA) v. 2.1.4. Geoscientific Model Development, 8(7), 1991–2007. https://doi.org/10.5194/gmd-8-1991-2015

[15] Westaway, R. M., Lane, S. N., & Hicks, D. M. (2000). The development of an automated correction procedure for digital photogrammetry for the study of wide, shallow, gravelbed rivers. Earth Surface Processes and Landforms 25(2), 209–226. https://doi.org/10.1002/(SICI)1096-9837(200002)25:2<209::AID-ESP84>3.0.CO;2-Z

[16] Wheaton, J. M., Brasington, J., Darby, S. E., & Sear, D. A. (2010). Accounting for uncertainty in DEMs from repeat topographic surveys: improved sediment budgets. Earth surface processes and landforms: the journal of the British Geomorphological Research Group, 35(2), 136-156. https://doi.org/10.1002/esp.1886

[17] Vergari, F., Troiani, F., Faulkner, H., Del Monte, M., Della Seta, M., Ciccacci, S., Fredi, P., 2019. The use of the slope–area function to analyse process domains in complex badland landscapes. Earth Surf. Process. Landf. 44, 273–286. https://doi.org/10.1002/esp.4496

[18] Neugirg, F., Stark, M., Kaiser, A., Vlacilova, M., Della Seta, M., Vergari, F., Schmidt, J., Becht, M., Haas, F. (2016). Erosion processes in calanchi in the Upper Orcia Valley, Southern Tuscany, Italy based on multitemporal high-resolution terrestrial LiDAR and UAV surveys. Geomorphology, 269, 8–22. https://doi.org/10.1016/j.geomorph.2016.06.027

[19] Stark M., Heckmann T., Piermattei L., Dremel F., Kaiser A., Machwski P., Haas F., and Becht M. (2021). From consumer to enterprise grade: How the choice of four UAS impacts point cloud quality. *Earth Surface Processes and Landforms* 46:2019–2043. https://doi.org/10.1002/esp.5142